



Universiteit  
Leiden  
The Netherlands

## The electrode-electrolyte interface in CO<sub>2</sub> reduction and H<sub>2</sub> evolution: a multiscale approach

Cecilio de Oliveira Monteiro, M

### Citation

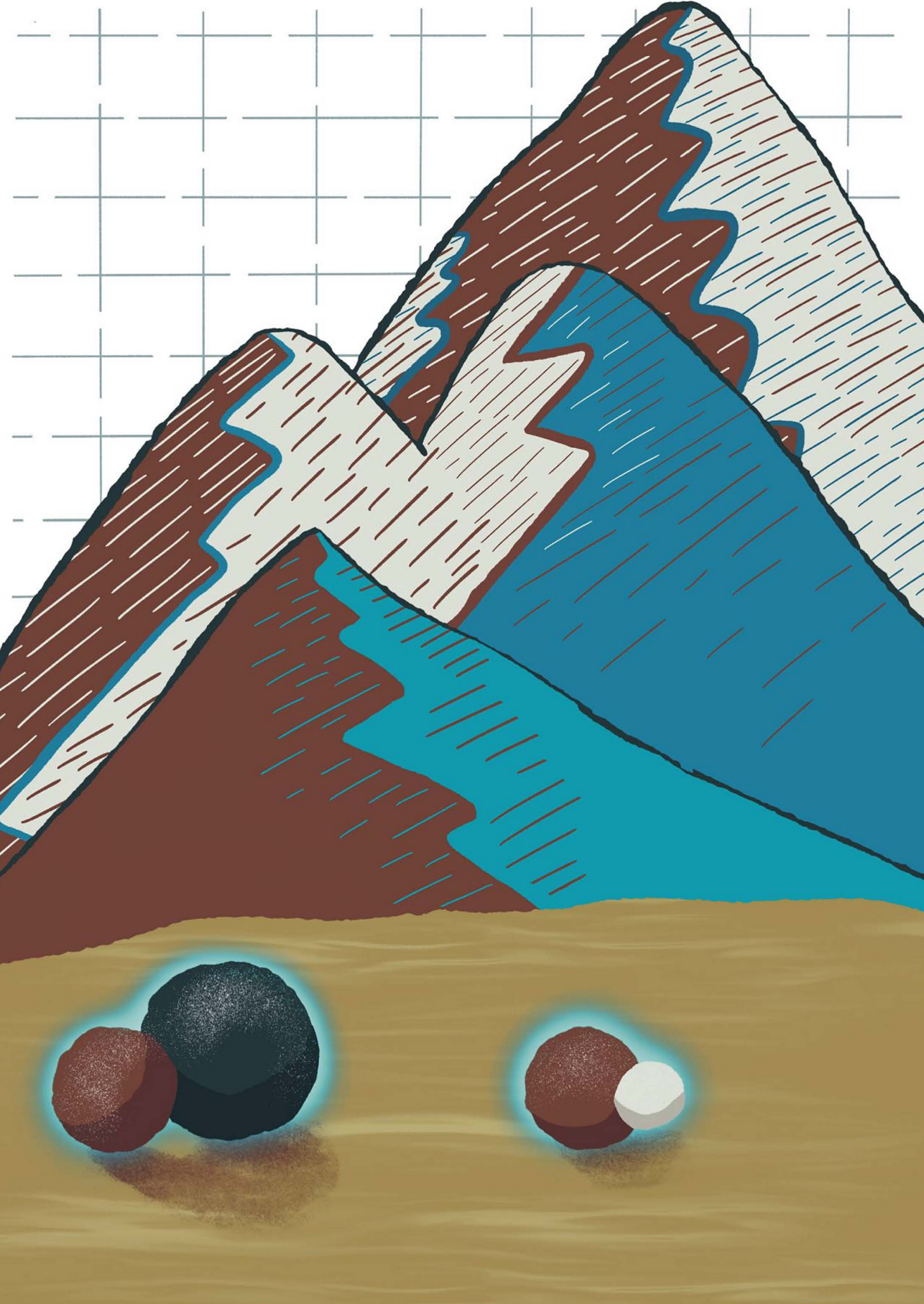
Cecilio de Oliveira Monteiro, M. (2022, February 15). *The electrode-electrolyte interface in CO<sub>2</sub> reduction and H<sub>2</sub> evolution: a multiscale approach*. Retrieved from <https://hdl.handle.net/1887/3274033>

Version: Publisher's Version

License: [Licence agreement concerning inclusion of doctoral thesis in the Institutional Repository of the University of Leiden](#)

Downloaded from: <https://hdl.handle.net/1887/3274033>

**Note:** To cite this publication please use the final published version (if applicable).



# 5

## Understanding the voltammetry of bulk CO electrooxidation in neutral media through combined SECM measurements

This chapter is based on Monteiro, M. C. O., Jacobse, L., Koper, M. T. M. *J. Phys. Chem. Lett.*, 11 (22), 9708–9713 (2020)

## Abstract

Recently, the bulk electrooxidation of CO on gold or platinum has been used to detect CO produced during CO<sub>2</sub> reduction in neutral media. The CO bulk oxidation voltammetry may show two distinct peaks depending on the reaction conditions, which up to now have not been understood. We have used Scanning Electrochemical Microscopy (SECM) to probe CO oxidation and pH in the diffusion layer during CO<sub>2</sub> reduction. Our results show that the two different peaks are due to diffusion limitation by two different species, namely CO and OH<sup>-</sup>. We find that between pH 7 and 11, CO oxidation by water and OH<sup>-</sup> gives rise to the first and second peak observed in the voltammetry, respectively. Additional rotating disc experiments showed that specifically in this pH range the current of the second peak is diffusion limited by the OH<sup>-</sup> concentration, since it is lower than the CO concentration.

## 5.1 Introduction

The electrochemical oxidation of CO on gold<sup>1–4</sup> and platinum<sup>5–9</sup> has been widely studied, especially how pH and surface structure affect the reaction.<sup>10–12</sup> Recently, CO oxidation on these two surfaces has been used in Rotating Ring Disc Electrode (RRDE)<sup>13–15</sup>, Scanning Electrochemical Microscopy (SECM)<sup>16,17</sup>, and cyclic voltammetry<sup>18</sup> experiments for in-situ probing the products of CO<sub>2</sub> reduction (CO<sub>2</sub>RR) or the interfacial pH. In these studies, mostly carried out in neutral media, two distinct or convoluted peaks have been observed in the CO oxidation voltammetry<sup>13,14,16–18</sup>, but their assignment is unclear. While the oxidation of a CO adlayer has been extensively studied on mono and polycrystalline platinum at different pH, there are no reports elucidating the mechanism of CO bulk oxidation on platinum in neutral media. These conditions are of special interest as the typical CO<sub>2</sub>RR reaction environment.

In general, the electrochemical oxidation of CO is believed to take place through a Langmuir–Hinshelwood mechanism, similar to the gas phase reaction. It is proposed that an adsorbed CO is oxidized by a nearest-neighbor oxygen containing species. The oxygen donor is generally believed to be OH<sub>ad</sub> from water in acidic (Eq. 5.1) or from OH<sup>–</sup> in alkaline (Eq. 5.2) media, respectively.<sup>19</sup>



Especially on gold electrodes, previous work has shown that CO oxidation takes place at higher overpotentials in acidic than in alkaline media.<sup>3</sup> As studies on bulk CO oxidation have previously been carried out only in strongly acidic or alkaline conditions, there is currently no consistent explanation for the coexistence of two peaks in the bulk CO electrooxidation voltammetry in neutral media.

Using platinum cyclic voltammetry to determine CO<sub>2</sub>RR products is a relatively new approach. Narayanaru et al.<sup>16</sup> used a platinum ultramicroelectrode (Pt-UME) in the substrate generation–tip collection (SG–TC) mode of SECM to probe the products of CO<sub>2</sub>RR on gold in 0.1 M KHCO<sub>3</sub> electrolyte. Two distinct CO oxidation peaks were observed in the Pt-UME voltammetry when the gold sample was held at –1.3 V vs. Ag/AgCl. Although a shift in the CO oxidation peak potential was observed as a function of sample roughness, and attributed to interfacial pH changes, the nature of the two different CO oxidation peaks was not discussed. In the same work, CO oxidation on gold directly after CO<sub>2</sub>RR was also performed and

two distinct anodic peaks were observed in the CO oxidation region. The authors attributed the peak at more positive potential to the oxidation of CO and the peak at less positive potential to the oxidation of methanol. Recently, Zhang and Co<sup>13</sup> reported the use of a RRDE with CO<sub>2</sub>RR performed on a gold disc while oxidation of the reaction products is carried out on a platinum ring. A broad CO oxidation peak is observed on the platinum ring, which seems actually a convolution of two different peaks. The broadness of the peak was explained by the presence of bubbles and not further discussed. In the same work, CO oxidation was carried out on the polycrystalline Pt ring in CO saturated 0.1 M KHCO<sub>3</sub> at pH 6.8 and 9.2. At pH 9.2 two distinct peaks were observed and attributed to CO oxidation taking place at {100} facets and {111} facets of the Pt-UME.

To better understand bulk CO oxidation in the CO<sub>2</sub>RR reaction environment, in this chapter, we have used a Pt-UME in the SG-TC mode of SECM while CO<sub>2</sub>RR was carried out at a gold substrate. Using the functionalized gold pH sensor from Chapter 3, we have used SECM to also measure the pH in the diffusion layer under the same reaction conditions and approximately same tip-to-surface distance.<sup>20</sup> The correlation of these results and additional Rotating Disc Electrode (RDE) measurements provide a clear understanding on the nature of the two different CO oxidation peaks previously observed<sup>13,14,16-18</sup>, and how they are influenced by the interfacial pH. Our measurements show the nature of the oxygen donor as a function of pH, and how in a narrow pH window the diffusion of these species and not (only) the diffusion of CO itself is what limits the current of the oxidation reaction and gives rise to the specific voltammetry. We emphasize that CO diffusion in this chapter refers to CO bulk diffusion, not to CO surface diffusion as it has been studied in CO stripping experiments.<sup>10,11</sup>

## 5.2 SECM CO oxidation measurements

To probe CO oxidation while CO<sub>2</sub>RR and the competing hydrogen evolution (HER) are taking place at the gold sample, a Pt-UME is used. A schematic representation of the experiment is shown in Fig. 5.1a. The blank and CO stripping cyclic voltammetry (CV) of the Pt-UME can be seen in Fig. 5.1c. The Pt-UME used here has a radius of approximately  $6.5 \pm 0.07 \mu\text{m}$ , determined with the Fe(CN)<sub>6</sub><sup>3-</sup>/Fe(CN)<sub>6</sub><sup>4-</sup> outer sphere reaction (see Fig. B.1 in Appendix B). After characterization<sup>20</sup> of the Pt-UME, a capacitive approach<sup>20,21</sup> is performed in air in order to determine the tip-to-surface distance. Fig. 5.1d shows a measured

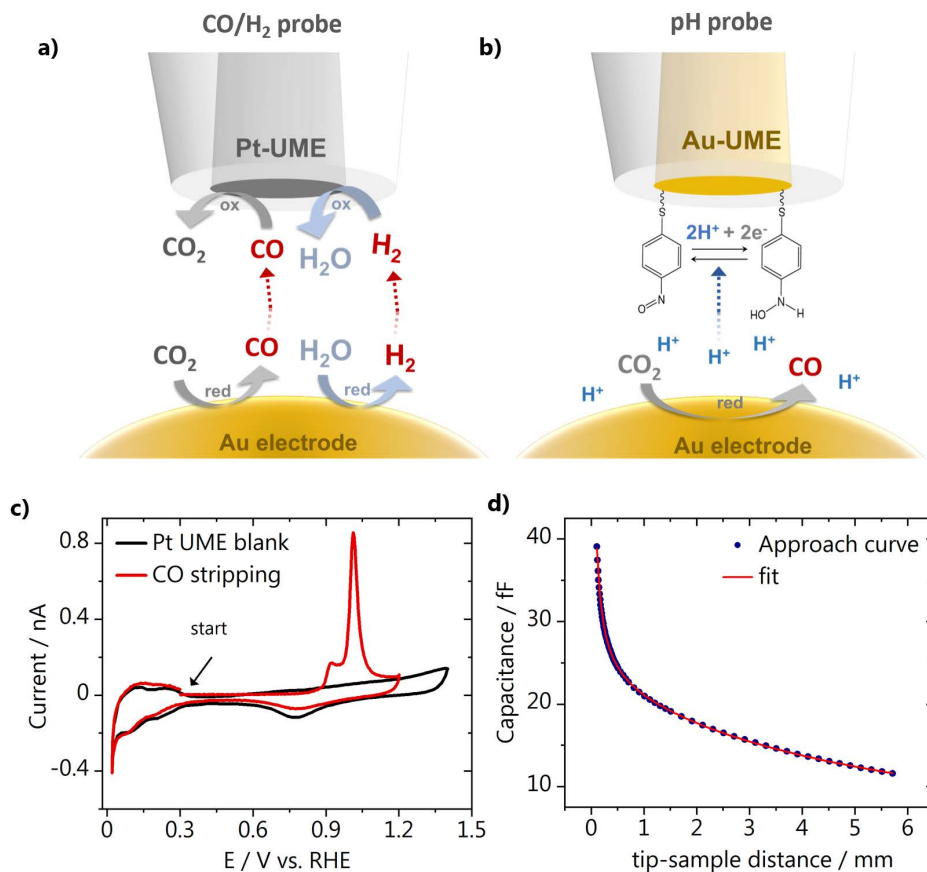


**Fig. 5.1.** Schematic representation of **a)** the SG-TC collection mode of SECM, where a Pt-UME is used to probe CO and H<sub>2</sub> while CO<sub>2</sub> reduction takes place at the gold sample, **b)** the functionalized Au-UME used to measure pH, **c)** Pt-UME blank voltammetry (black) taken in argon saturated 0.1 M H<sub>2</sub>SO<sub>4</sub> and CO stripping voltammetry measured in the same electrolyte after exposing the Pt-UME to a CO atmosphere for 5 minutes. CVs taken at 200 mV s<sup>-1</sup>. **d)** Capacitive approach curve to determine the absolute tip-to-surface distance.

approach curve (data points) together with its fit (line). Details on the capacitive approach curve measurement and fitting are available in Chapter 3 and Appendix B (Fig. B.2). To minimize the influence of the tip in the diffusion process, it was placed at a relatively large distance of  $40 \pm 3 \mu\text{m}$  from the surface.

During CO<sub>2</sub>RR, the composition of the reaction interface changes significantly due to OH<sup>-</sup> generation. Consequently, the local pH depends on the sample potential. To investigate the nature of the two distinct peaks in the bulk CO oxidation voltammetry, we have created different CO<sub>2</sub>RR reaction environments

around the Pt-UME, by using an unbuffered electrolyte (0.1 M  $\text{Cs}_2\text{SO}_4$ , pH = 3) and changing the potential at which the reaction is carried out at the gold substrate.

The Pt-UME voltammetry is constantly recorded while chronoamperometry at the sample is carried out at different potentials. The chronoamperometry data from the gold sample can be found in Fig. B.3 in Appendix B. Fig. 5.2 shows the results obtained at different sample potentials. Ten cycles of the Pt-UME were recorded, and the 10<sup>th</sup> cycle is displayed. It can be seen that at low sample potentials (Fig. 5.2a) only hydrogen is produced at the gold sample as the tip voltammetry shows features characteristic of hydrogen oxidation (HOR).<sup>22</sup> The HOR current increases when going from -0.1 to -0.3 V but stops increasing between -0.3 and -0.4 V likely due to diffusion limitation of the proton reduction reaction taking place at the surface. At these potentials, no strong pH gradients are expected and bicarbonate is present only in trace amounts, as the  $\text{pK}_a$  of the  $\text{CO}_{2(\text{aq})} + \text{H}_2\text{O} \rightleftharpoons \text{HCO}_3^- + \text{H}^+$  equilibrium reaction is 6.4. At -0.5 V (sample potential) CO starts being formed. This leads to the poisoning of the Pt-UME for HOR, and a small CO oxidation peak appears in the forward scan (see Fig. 5.2b). This peak gradually increases and shifts slightly positive going from -0.5 to -0.65 V, due to a higher concentration of CO in solution. For simplicity, from now on we will call this "peak I". In the backward scan, a peak due to HOR is still observed at sample potentials -0.5 and -0.55 V, which decreases due to the increase in CO concentration. At -0.6 and -0.65 V only current due to bulk CO oxidation is seen at the Pt-UME voltammetry and a subtle shoulder appears, which we will call "peak II". The shape of the CO oxidation CV with the hysteresis between forward and backward scans is typical for bulk CO oxidation on Pt, and discussed in detail elsewhere.<sup>23</sup>

Fig. 5.2c shows results obtained at sample potentials -0.7 and -0.75 V. At -0.7 V the CO oxidation peak shows a clear shoulder in the Pt-UME voltammetry at 0.45 V vs. Ag/AgCl due to an increase of peak II. At -0.75 V peak II gradually increases while peak I decreases. Here, three subsequent Pt-UME CVs are plotted to show this peak I/peak II transition. This transition suggests a strong change in the reaction environment when -0.75 V is applied to the gold sample. If the rate of  $\text{OH}^-$  production becomes higher than the rate at which bicarbonate can be formed, the alkalinity near the surface will increase and the concentration of  $\text{OH}^-$  will become larger than the concentration of  $\text{HCO}_3^-$ . The coexistence of peak I and peak II strongly suggests that two different mechanisms for CO oxidation are taking place

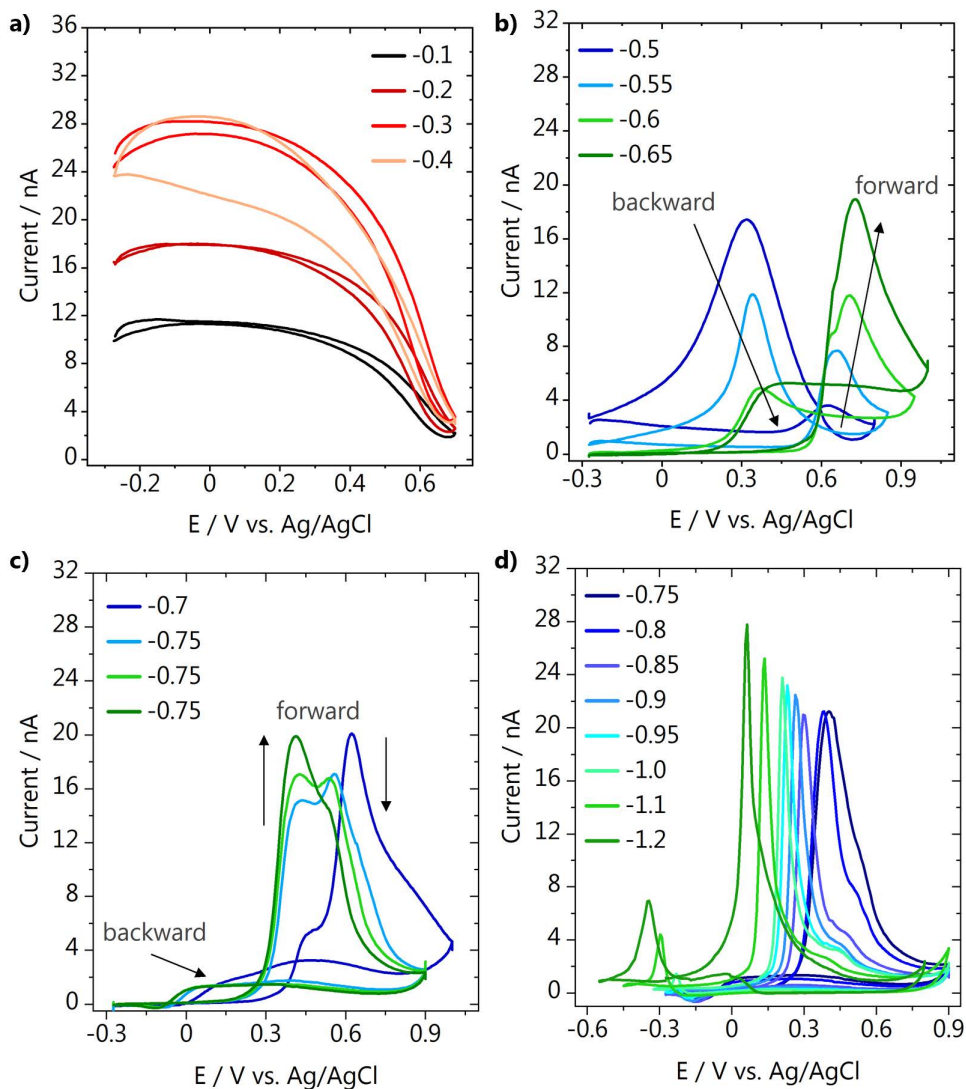


**Fig. 5.2.** Pt-UME voltammetry recorded in 0.1 M Cs<sub>2</sub>SO<sub>4</sub> (200 mV s<sup>-1</sup>, pH = 3) while CO<sub>2</sub>RR and/or HER take place at the gold sample at potentials **a)** from -0.1 to -0.4 V, **b)** from -0.5 to -0.65 V, **c)** from -0.7 to -0.75 V and **d)** from -0.75 to -1.2 V. The gold sample potentials shown in the legend are reported versus the reversible hydrogen electrode.

simultaneously as a function of the reaction environment, i.e.  $\text{OH}^-$  concentration. At more negative sample potentials, it can be seen in the Pt-UME voltammetry (Fig. 5.2d) that peak I is still present, but gradually becomes less pronounced. Peak II shifts to more negative potentials, likely due to an increase in local alkalinity. At  $-1$  V sample potential, a small peak appears in the backward scan at  $-0.23$  V vs. Ag/AgCl due to hydrogen oxidation.

To better understand the mechanism behind bulk CO oxidation and the diffusion processes taking place, the currents of peak I and peak II are evaluated separately by holding the gold sample at potentials where either peak I or peak II are present ( $-0.65$  and  $-0.9$  V vs. RHE). By varying the scan rate at which the Pt-UME voltammetry is recorded, we can gain insights into the nature of the species participating in the reaction and limiting the current, as the peak current can be calculated following the Randles-Sevcik equation<sup>24</sup>:

$$i_p = 2.69 * 10^5 * n^{3/2} * A * D^{1/2} * C * \nu^{1/2} \quad \text{Eq. 5.4}$$

where  $n$  is the number of electrons transferred,  $A$  is the electrode surface area,  $D$  is the diffusion coefficient of the reacting species that limits the current and  $C$  its concentration, and  $\nu$  is the scan rate. The peak current plotted as a function of the square root of the scan rate can be seen in Fig. 5.3. The two different slopes

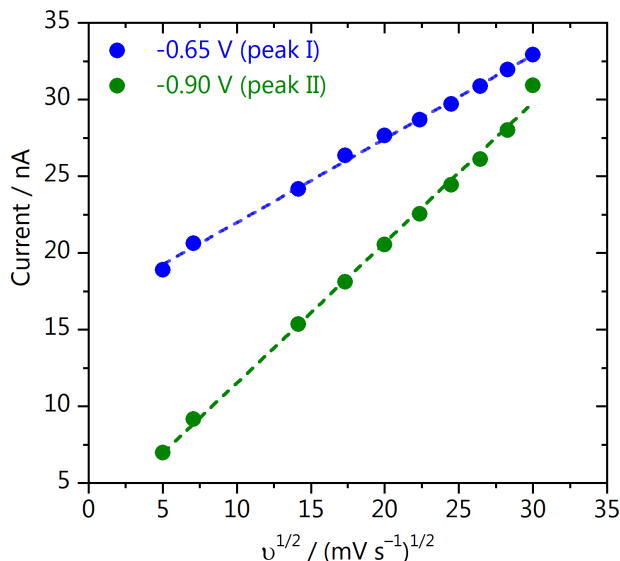


**Fig. 5.3.** Scan rate dependency of the CO oxidation peak current measured at the Pt-UME. Measurements were performed at two different sample potentials to evaluate separately the CO oxidation peak I (blue) and peak II (green).

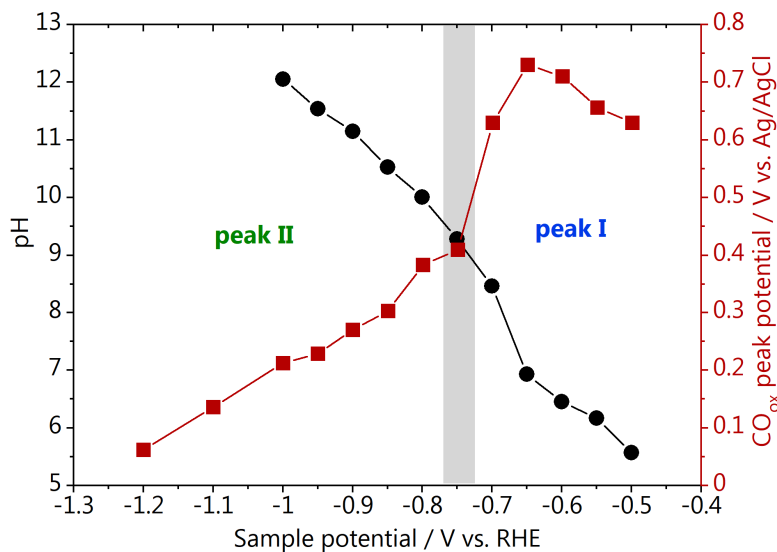


**Fig. 5.4.** Correlation between the pH measurements performed with a functionalized Au-UME (black circles) with the CO oxidation peak position extracted from the measurements performed with the Pt-UME (red squares) during CO<sub>2</sub> reduction on gold (0.1 M Cs<sub>2</sub>SO<sub>4</sub>, pH = 3, CO<sub>2</sub> saturated).

found indicate that the reaction is limited by the diffusion of two different species, giving rise to the two observed peaks in the voltammetry. However, derivation of the diffusion coefficient for identification of the species is not possible here, as the exact concentration of the reactants is unknown.

### 5.3 SECM local pH measurements

To gain better insights into the reaction interface when these two peaks coexist, SECM pH measurements were performed under the same conditions as the previously shown H<sub>2</sub>/CO oxidation experiments. Here, the tip is a functionalized gold ultramicroelectrode (Au-UME) pH sensor. The Au-UME used here has a radius of approximately  $26.9 \pm 0.05 \mu\text{m}$ , determined with the Fe(CN)<sub>6</sub><sup>3-</sup>/Fe(CN)<sub>6</sub><sup>4-</sup> outer sphere reaction (see Fig. B.1 in Appendix B). As can be seen in the scheme in Fig. 5.1b the gold surface is modified with a self-assembled monolayer containing the hydroxylaminothiophenol/4-nitrosothiophenol redox couple. The pH sensing is realized by recording the tip cyclic voltammetry and monitoring the Nernstian shift of the midpeak potential. Details on the sensor fabrication and data processing can be found in Chapter 3, Appendix A and Appendix B.<sup>20</sup> The Au-UME is positioned at

the same distance from the surface as the Pt-UME ( $40 \pm 3 \mu\text{m}$ ) and the tip voltammetry is recorded while changing the sample potential. The pH measurements in time can be found in Fig. B.4 in the Appendix B. The measured pH as a function of sample potential is displayed in Fig. 5.4 together with the peak potential of the CO oxidation peaks from Fig. 5.2. At low sample potentials neither the pH increases, nor the CO oxidation peak I shifts negatively. In this potential range the  $\text{CO}_{2(\text{aq})} \rightleftharpoons \text{HCO}_3^-$  equilibrium buffers the interfacial pH, which value remains near the  $\text{pK}_a$  of the equilibrium reaction (6.4). At  $-0.75 \text{ V}$  sample potential, where the transition between peak I and peak II is observed (Fig. 5.2c), there is an increase in pH from 7.7 to 9 and the CO oxidation peak also starts to shift negatively. The correlation showed in Fig. 5.4 suggests that peak I exists at neutral pH, and therefore water is the oxygen donor for CO oxidation. As peak II appears when the buffer breaks down and the interface becomes more alkaline, it seems that peak II corresponds to CO being oxidized by  $\text{OH}^-$ . However, these findings still do not elucidate why different slopes were found in Fig. 5.3, which suggests that the current of peak I and II is limited by two different species, which could be:  $\text{OH}^-$ , CO, or  $\text{HCO}_3^-$ .

#### 5.4 Rotating Disc Electrode (RDE) experiments

To assign the species leading to the diffusion limiting current observed for peak I and II, we performed rotating disc electrode (RDE) experiments using a polycrystalline platinum disc. The blank voltammetry of the platinum electrode is seen in Fig. B.6 in Appendix B. Fig. 5.5 displays the results obtained in pure  $0.1 \text{ M Cs}_2\text{SO}_4$  ( $\text{pH} = 7.2$ ) and when  $0.03$ ,  $0.06$  and  $1 \text{ mM}$  of KOH are added to the electrolyte, leading to  $\text{pH}$   $9.5$ ,  $9.8$  and  $11$ , respectively. The electrolyte is saturated with CO during all the measurements, leading to a constant CO concentration of  $1 \text{ mM}$ . Fig. 5.5a shows the voltammetry of bulk CO oxidation in the different electrolytes taken at  $400 \text{ rpm}$ . In pure  $\text{Cs}_2\text{SO}_4$  (neutral pH) only one diffusion limiting plateau is seen between  $1.2$  and  $1.6 \text{ V}$  vs. RHE, corresponding to peak I previously observed in the SECM measurements. When  $0.03 \text{ mM}$  KOH is added to the electrolyte, two plateaus are observed. One with a similar current as before, between  $1.2$  and  $1.6 \text{ V}$  vs. RHE, and another with lower diffusion limiting current, between  $0.8$  and  $1.2 \text{ V}$  vs. RHE (peak II). Increasing the  $\text{OH}^-$  concentration leads to an increase in the diffusion limiting current of peak II, confirming the correlation found in the SECM measurements between peak II and pH. At  $\text{pH}$   $11$  ( $1 \text{ mM}$  KOH), only one peak is observed at lower overpotentials, with a current matching the one

found at pH 7.2. To elucidate which species cause diffusion limitation in each condition, measurements were also performed at different rotation rates (see Fig. B.7 in Appendix B). The Levich equation describes the relationship between the diffusion limiting current and the rotation rate and can be used to derive the diffusion coefficient of the species leading to the diffusion limitation:<sup>24</sup>

$$j_{lim} = 0.62 * n * F * D^{2/3} * \nu^{-1/6} * C * \omega^{1/2} \quad \text{Eq. 5.5}$$

where  $n$  is the number of electrons transferred,  $F$  is the Faraday constant,  $D$  is the diffusion coefficient of the species,  $\nu$  is the kinematic viscosity of the solvent,  $C$  is

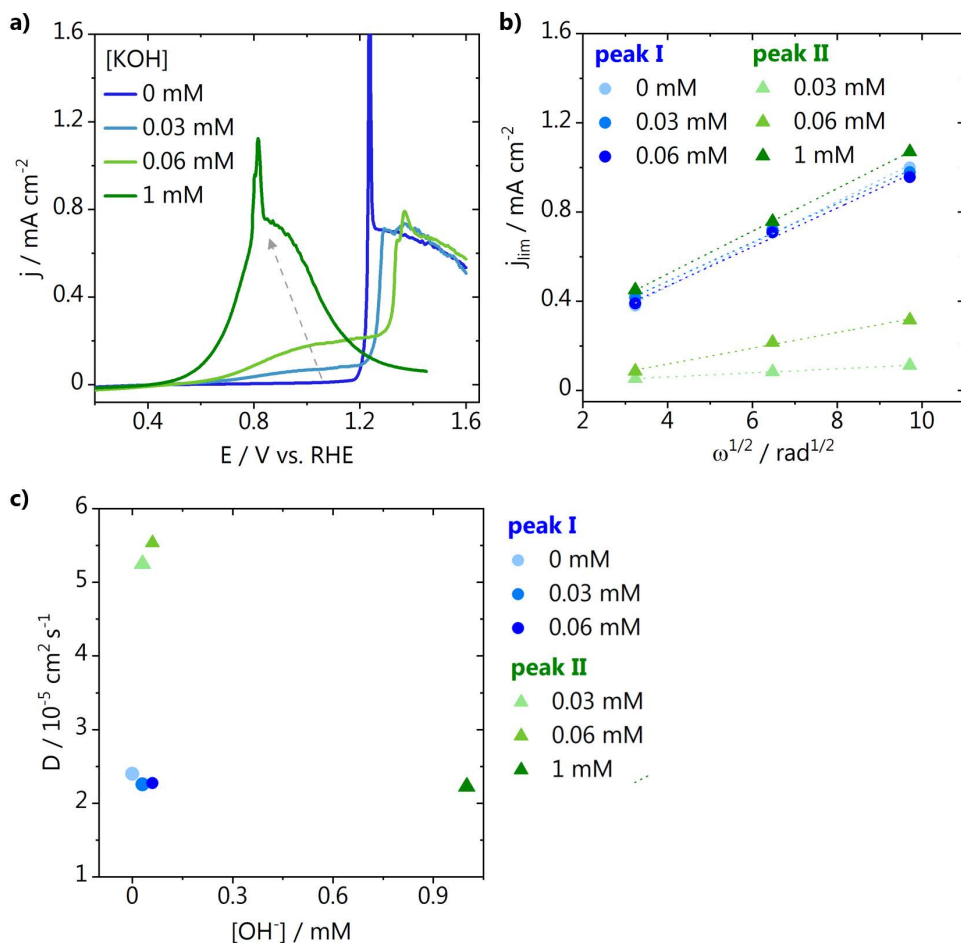


**Fig. 5.5.** RDE CO oxidation measurements on a polycrystalline Pt disc in Cs<sub>2</sub>SO<sub>4</sub> (pH = 7.2) performed at 400 rpm with 25 mV s<sup>-1</sup> scan rate. **a)** Reaction performed in the presence of different concentrations of KOH, **b)** Levich plot and **c)** derivation of the diffusion coefficients for peak I (blue circles) and peak II (green triangles).

the concentration of the species and  $\omega$  is the rotation rate. The diffusion limiting currents obtained at the different rotations for the plateaus corresponding to peak I and II are shown in Fig. 5.5b as a function of the square root of the rotation rate. The diffusion coefficients are derived from the slopes obtained in Fig. 5.5b and are displayed in Fig. 5.5c. It can be seen that for peak I, the same slope is found in pure  $\text{Cs}_2\text{SO}_4$  and in the presence of 0.03 and 0.06 mM of  $\text{OH}^-$ . The diffusion coefficients calculated all approximate the theoretical value reported for CO which is  $2.03 \cdot 10^{-5} \text{ cm}^2 \text{ s}^{-1}$ , confirming that the current of peak I is limited by the diffusion of CO.<sup>25</sup> In the case of peak II, interestingly, a different slope is found as a function of the  $\text{OH}^-$  concentration. When the  $\text{OH}^-$  concentration is lower than the CO concentration (1 mM), a slope of approximately  $5.5 \cdot 10^{-5} \text{ cm}^2 \text{ s}^{-1}$  is found based on the  $\text{OH}^-$  concentration, corresponding to the value reported for  $\text{OH}^-$  ions ( $5.23 \cdot 10^{-5} \text{ cm}^2 \text{ s}^{-1}$ ).<sup>25</sup> This clearly shows that in this pH range,  $\text{OH}^-$  is not only the oxygen donor but also the species whose transport limits the reaction. When the  $[\text{OH}^-] = [\text{CO}] = 1\text{mM}$  the slope found is similar to the one of peak I and derivation of the diffusion coefficient based on the CO concentration again matches the value reported in literature for CO. The latter implies that at pH 11 or higher, only one peak is present, and the current is limited by the diffusion of CO.

## 5.5 Discussion and Conclusions

Based on the two different SECM measurements and the RDE results, we can now build a clear understanding of the nature of the two peaks observed during bulk CO electrooxidation in neutral media. As summarized in Table 5.1, at acidic and neutral pH,  $\text{OH}^-$  is present in small concentrations and CO is oxidized by water. The current is limited by the concentration of CO in solution and only one peak is observed in the voltammetry at high overpotential: peak I. Between pH 7 and 11, two peaks coexist in the CO oxidation voltammetry: peak I and peak II. Peak II appears at lower overpotentials than peak I and is due to CO oxidation by  $\text{OH}^-$ . The current is limited by the  $\text{OH}^-$  concentration. Above pH 11, only peak II is present due to CO oxidation by  $\text{OH}^-$ , and the current is limited again by the concentration of CO, which becomes smaller than the  $\text{OH}^-$  concentration in this pH range. Even though methanol has been previously observed as a product of  $\text{CO}_2$  reduction on roughened gold electrodes<sup>16</sup>, we can exclude that methanol oxidation gives rise to peak II. We have analyzed the  $\text{CO}_2\text{RR}$  products formed in the conditions of this study (flat gold electrode, 0.1 M  $\text{Cs}_2\text{SO}_4$ , pH = 3) with online chromatography

**Table 5.1.** Relationship between pH,  $j_{\text{lim}}$  species and the bulk CO electrooxidation voltammetry.

pH	O-donor	$j_{\text{lim}}$ species	voltammetry
$\leq 7$	H <sub>2</sub> O	CO	peak I
$11 > \text{pH} > 7$	H <sub>2</sub> O, OH <sup>-</sup>	OH <sup>-</sup>	peak I + peak II
$\geq 11$	OH <sup>-</sup>	CO	peak II

(Fig. B.8 in Appendix B). The only products detected are hydrogen and CO, at potentials for which peak I and II are observed.

Summarizing, in the present work we have used SECM in SG-TC mode to probe CO oxidation on a Pt-UME while CO<sub>2</sub>RR to CO takes place on a gold sample. By changing the local reaction environment, we could observe the existence of two distinct peaks in the CO oxidation voltammetry as a function of pH. SECM local pH measurements were also performed demonstrating a clear correlation between the OH<sup>-</sup> concentration and the coexistence of the two distinct CO oxidation peaks. Additional RDE measurements confirmed that the peaks coexist in a narrow pH range in which the OH<sup>-</sup> concentration is smaller than the CO concentration (between pH 7 and 11), which results in two diffusion limited current regimes. It is now clear why these two peaks are mainly observed when probing CO<sub>2</sub> reduction<sup>13,14,16-18</sup>, as the pH in the CO<sub>2</sub> reduction reaction environment usually lies in between the CO<sub>2</sub>/HCO<sub>3</sub><sup>-</sup> pK<sub>a</sub> and more alkaline values that develop according to the current density and buffer capacity of the electrolyte used. Considering the increased number of publications where CO oxidation is being used to probe CO<sub>2</sub> reduction, we hope the work presented in this Chapter provides the basis for the correct assignment of the two distinct peaks often observed in the CO oxidation voltammetry.

## References

- (1) Kita, H.; Nakajima, H.; Hayashi, K. *J. Electroanal. Chem.* 1985, *190* (1–2), 141–156.
- (2) Rodriguez, P.; Garcia-Araez, N.; Koper, M. T. M. *Phys. Chem. Chem. Phys.* 2010, *12* (32), 9373–9380.
- (3) Rodriguez, P.; Koper, M. T. M. *Phys. Chem. Chem. Phys.* 2014, *16* (27), 13583–13594.
- (4) Rodriguez, P.; Plana, D.; Fermin, D. J.; Koper, M. T. M. *J. Catal.* 2014, *311*, 182–189.
- (5) Grgur, B. N.; Marković, N. M.; Lucas, C. A.; Ross, P. N. *J. Serbian Chem. Soc.* 2001, *66* (11–12), 785–797.
- (6) Kita, H.; Shimazu, K.; Kunimatsu, K. *J. Electroanal. Chem.* 1988, *241* (1–2), 163–179.
- (7) Abe, K.; Uchida, H.; Inukai, J. *Surfaces* 2019, *2* (2), 315–325.
- (8) Park, I. S.; Chen, D. J.; Atienza, D. O.; Tong, Y. J. *Catal. Today* 2013, *202* (1), 175–182.
- (9) Wang, H.; Abruña, H. D. *J. Phys. Chem. Lett.* 2015, *6* (10), 1899–1906.
- (10) Lai, S. C. S.; Lebedeva, N. P.; Housmans, T. H. M.; Koper, M. T. M. *Top. Catal.* 2007, *46* (3–4), 320–333.
- (11) García, G.; Koper, M. T. M. *ChemPhysChem* 2011, *12* (11), 2064–2072.
- (12) Gisbert, R.; García, G.; Koper, M. T. M. *Electrochim. Acta* 2011, *56* (5), 2443–2449.
- (13) Zhang, F.; Co, A. C. *Angew. Chemie Int. Ed.* 2020, *59* (4), 1674–1681.
- (14) Zhang, F.; Co, A. C. *J. Electrochem. Soc.* 2020, *167* (4), 046517.
- (15) Goyal, A.; Marcandalli, G.; Mints, V. A.; Koper, M. T. M. *J. Am. Chem. Soc.* 2020, *2* (1), 4154–4161.
- (16) Narayanaru, S.; Chinnaiyah, J.; Phani, K. L.; Scholz, F. *Electrochim. Acta* 2018, *264*, 269–274.
- (17) Sreekanth, N.; Phani, K. L. *Chem. Commun.* 2014, *50* (76), 11143–11146.
- (18) Lee, C. W.; Cho, N. H.; Nam, K. T.; Hwang, Y. J.; Min, B. K. *Nat. Commun.* 2019, *10* (1), 1–8.
- (19) McPherson, I. J.; Ash, P. A.; Jones, L.; Varambhia, A.; Jacobs, R. M. J.; Vincent, K. A. *J. Phys. Chem. C* 2017, *121* (32), 17176–17187.
- (20) Monteiro, M. C. O.; Jacobse, L.; Touzalin, T.; Koper, M. T. M. *Anal. Chem.* 2020, *92* (2), 2237–2243.
- (21) Voogd, J. M. De; Spronsen, M. A. Van; Kalff, F. E.; Bryant, B.; Ostojji, O.; Haan, A. M. J. Den; Groot, I. M. N.; Oosterkamp, T. H.; Otte, A. F.; Rost, M. J. *Ultramicroscopy* 2017, *181*, 61–69.
- (22) Sheng, W.; Zhuang, Z.; Gao, M.; Zheng, J.; Chen, J. G.; Yan, Y. *Nat. Commun.* 2015, *6*, 6–11.
- (23) Koper, M. T. M.; Schmidt, T. J.; Marković, N. M.; Ross, P. N. *J. Phys. Chem. B* 2001, *105* (35), 8381–8386.
- (24) Bard, A. J.; Faulkner, L. R. 2nd ed.; John Wiley & Sons, 2001.
- (25) Haynes, W. M. 95th ed.; CRC Press: New York, 2014.

